J. Adv. Model. Earth Syst., **Vol. 1**, Art. #15, 13 pp.

Large-Eddy Simulation of Maritime Deep Tropical Convection

Marat F. Khairoutdinov[1], Steve K. Krueger[2], Chin-Hoh Moeng[3], Peter A. Bogenschutz[2] and David A. Randall[4]

[1] School of Marine and Atmospheric Sciences, Stony Brook University, Stony Brook, New York
[2] Department of Atmospheric Sciences, University of Utah, Salt Lake City, Utah
[3] Mesoscale & Microscale Meteorology Division, National Center for Atmospheric Research, Boulder, Colorado
[4] Department of Atmospheric Science, Colorado State University, Fort Collins, Colorado

Manuscript submitted 16 October 2009; Revised 18 December 2009

This study represents an attempt to apply Large-Eddy Simulation (LES) resolution to simulate deep tropical convection in near equilibrium for 24 hours over an area of about 205 × 205 km^2, which is comparable to that of a typical horizontal grid cell in a global climate model. The simulation is driven by large-scale thermodynamic tendencies derived from mean conditions during the GATE Phase III field experiment. The LES uses 2048 × 2048 × 256 grid points with horizontal grid spacing of 100 m and vertical grid spacing ranging from 50 m in the boundary layer to 100 m in the free troposphere. The simulation reaches a near equilibrium deep convection regime in 12 hours. The simulated vertical cloud distribution exhibits a tri-modal vertical distribution of deep, middle and shallow clouds similar to that often observed in Tropics. A sensitivity experiment in which cold pools are suppressed by switching off the evaporation of precipitation results in much lower amounts of shallow and congestus clouds. Unlike the benchmark LES where the new deep clouds tend to appear along the edges of spreading cold pools, the deep clouds in the no-cold-pool experiment tend to reappear at the sites of the previous deep clouds and tend to be surrounded by extensive areas of sporadic shallow clouds. The vertical velocity statistics of updraft and downdraft cores below 6 km height are compared to aircraft observations made during GATE. The comparison shows generally good agreement, and strongly suggests that the LES simulation can be used as a benchmark to represent the dynamics of tropical deep convection on scales ranging from large turbulent eddies to mesoscale convective systems.

The effect of horizontal grid resolution is examined by running the same case with progressively larger grid sizes of 200, 400, 800, and 1600 m. These runs show a reasonable agreement with the benchmark LES in statistics such as convective available potential energy, convective inhibition, cloud fraction, precipitation rates, and surface latent and sensible fluxes. All runs reveal a tri-model cloud distribution in the vertical. However, there are differences in the updraft-core cloud statistics, and convergence of statistical properties is found only between the LES benchmark and the run with 200 m grid size. The effect of vertical grid resolution is also investigated with another run that uses a typical cloud-resolving model (CRM) horizontal grid size on the order of 1 km and only 64 vertical levels. A comparison to the run with 256 vertical levels shows different vertical cloud distributions. It is concluded that representation of the often observed tri-modal vertical distribution of clouds requires a vertical grid spacing in the range of 50-100 m in mid-to-low troposphere.

DOI:10.3894/JAMES.2009.1.15

1. Introduction

Clouds remain primary contributors to uncertainties in numerical prediction of future climate change due to greenhouse gas emissions (IPCC, 2007). The Tropics occupy about half of the Earth's surface and hold most of the major greenhouse gas, water vapor, thus playing a key role in climate feedbacks involving water. Tropical cloudiness is

To whom correspondence should be addressed.
Marat Khairoutdinov, School of Marine and Atmospheric Sciences, Stony Brook University, Stony Brook, NY 11794-5000, USA
mkhairoutdin@ms.cc.sunysb.edu

usually the result of convection, sometimes chaotic and disorganized, but, depending on large-scale conditions, often organized into large convective systems. Tropical convective systems consist of individual clouds with a great variety of sizes and depths, from heavily precipitating deep convection and associated extensive upper tropospheric stratiform clouds to relatively small congestus and shallow cumuli. Clouds of different types, organized or not, often co-exist in close proximity, interacting in complicated ways. In addition, clouds interact with the large-scale circulation, the planetary boundary layer (PBL), radiation, etc. Ideally, this complexity should be represented in some statistical form in global climate models (GCMs). However, the *parameterization*, or statistical representation of unresolved-by-grid, so-called sub-grid scale (SGS), processes, is a longstanding problem, and is still far from being solved (e.g., Randall et al. 2003).

It is not possible to design a field experiment that could observe all the details of cloud-scale processes and interactions over an area comparable to a typical GCM grid size (on the order of a hundred kilometers). As an alternative, three-dimensional numerical models constrained by observations can be used. For example, large-eddy simulation models (LES) and cloud-resolving models (CRM) have been used extensively over the past two decades as virtual *testbeds* for parameterization development and process studies to better understand how clouds 'work' and interact with each other and with their environment (e.g., Randall et al. 2003).

The LES technique has been used to simulate turbulence and low clouds in the PBL, where the grid spacing (from meters to a hundred meters) typically lies within the Kolmogorov inertial sub-range of turbulence so the SGS fluxes can be estimated based on Kolmogorov theory (e.g., Moeng and Wyngaard 1988). Until very recently, computational limitations have constrained the LES applications to simulations of the PBL turbulence and low-level shallow clouds with relatively small horizontal domains of just a few kilometers in size (e.g., Siebesma et al. 2003; Stevens et al. 2005). On the other hand, CRMs have been the primary tools to study deep convective clouds and convective cloud systems (e.g., Klemp and Wilhelmson 1978; Tao and Soong 1986; Redelsperger and Sommeria 1986; Krueger 1988; Grabowski et al. 1998; Khairoutdinov and Randall 2003) with the typical numerical domain sizes on the order of hundreds of kilometers. Recently, it has become possible to study organized tropical convection using a global CRM (Nasuno et al. 2007). Yet again, due to computational limitations, CRMs have typically been run with horizontal grid sizes of 1-2 km. At that resolution, the boundary-layer turbulence and shallow clouds are under-resolved, so their effects have to be parameterized. Most CRMs adopt the same SGS schemes as those used in LES; however, since the grid size of CRMs is typically much larger than the inertial-subrange scale, the use of inertial-subrange-based SGS parameterizations in CRMs is less justified.

The gap between LES and CRMs is steadily closing, primarily because of rapid advances in massively parallel supercomputing. Nevertheless, so far, there have been only a few LES studies of deep convection with a horizontal grid spacing of O(100 m). Bryan et al. (2003) simulated a mid-latitude squall-line with 100 m horizontal grid spacing; they showed no convergence of statistical properties between the simulations with horizontal grid sizes of 100 and 250 m. Petch et al. (2002) also applied 100 m grid spacing to simulate the diurnal cycle of convection over land, although using a relatively small domain; they also reported no sign of convergence at high resolution. Khairoutdinov and Randall (2006) applied the model used in the present study to the problem of the shallow-to-deep transition over Amazonia using a 154×154 km^2 domain; they reported that the details of the transition were virtually indistinguishable between the runs with 100 and 250 m horizontal grid spacing.

In this paper, we present a 24-hour long LES of deep tropical convection over a domain of 204.8 km in both horizontal directions using the mean sounding and forcing observed during the GATE[1] Phase III experiment over the Atlantic Inter-Tropical Convergence Zone (ITCZ). Because it used one billion grid cells, the simulation has been nicknamed the 'Giga-LES'. This LES of deep tropical convection in the ITCZ covers a wide range of scales of motion, from energy-containing turbulent eddies to mesoscale circulations, in a domain comparable to a typical GCM grid cell.

The motivation for the 'Giga-LES' is to create a *benchmark* simulation, a sort of 'virtual field campaign', to 1) study details of scale interactions among PBL turbulence, shallow/congestus and deep convection, with associated cold pools, 2) examine sensitivity of cloud properties to the grid resolution typically used in CRMs, and 3) improve SGS representations in CRMs. This paper will look at resolution issues and the importance of cold pools for mid-level and shallow convection, while a companion paper, Moeng et al. (2009) uses the Giga-LES to examine an SGS representation commonly used in CRMs.

The paper is organized as follows. The model is described briefly in Section 2. Section 3 provides details of the case setup and model configuration. Section 4 describes the basic evolution of the benchmark LES run. Section 5 illustrates the effect of cold pools on the amount of shallow and mid-level convection. Section 6 compares the vertical velocity statistics to aircraft observations. Section 7 shows the results of grid resolution sensitivity tests. A brief summary of the findings is offered in Section 8.

2. Model description

The model used in this study is the System for Atmospheric Modeling (SAM; version 6.7) documented by Khairoutdinov and Randall (2003). The CRM solves the

[1] Global Atmospheric Research Program (GARP) Atlantic Tropical Experiment

anelastic system of momentum equations. The prognostic thermodynamic energy variable is the liquid/ice water moist static energy. It is conserved in all adiabatic and water-phase transformation processes but not for gravitational sedimentation. The two prognostic water variables are the total precipitation (sum of rain, snow and graupel) and the total non-precipitation (sum of water vapor, cloud liquid water and cloud ice) water mixing ratios. The main difference between the cloud water and precipitation in the model is that the cloud water exists only when a grid volume reaches a 100% relative humidity and is diagnosed using a simple iterative algorithm. It is computationally challenging to perform the high-resolution cloud simulations presented in this study because of the expensive positive-definite and monotonic numerical algorithm used for transport. Packing six water variables into just two composite prognostic variables speeds up the model performance by at least a factor of two.

The sub-grid scale (SGS) fluxes can be parameterized using a 1.5-order closure based on the prognostic SGS turbulent kinetic energy (TKE) equation following Deardorff (1980); however, in this study, the TKE was diagnosed from the quasi-steady TKE budget. The lateral boundary conditions in both horizontal directions are periodic while the upper boundary is a rigid lid. To reduce gravity-wave reflection and build-up above the tropopause, a Newtonian damping layer is applied above 19 km, with a damping time scale varying from 2 hours at 19 km to 2 min at the domain top.

3. Simulation setup

Figure 1 illustrates the initial thermodynamic profiles and large-scale forcing used in this study. They represent idealized mean conditions during the GATE Phase III field experiment, and were also used by Xu et al. (1992) and Fu et al. (1995). The prescribed large-scale advective and radiative cooling, and advective moistening tendencies were applied continuously and homogeneously in the horizontal. The surface latent, sensible, and momentum fluxes were computed. The sea surface temperature was fixed at 299.88 K. The domain-averaged horizontal wind profile was relaxed towards the prescribed profile with a 2-hour timescale. No nudging was done to any thermodynamic field during the 24-hour simulation. As illustrated in Fig. 1,

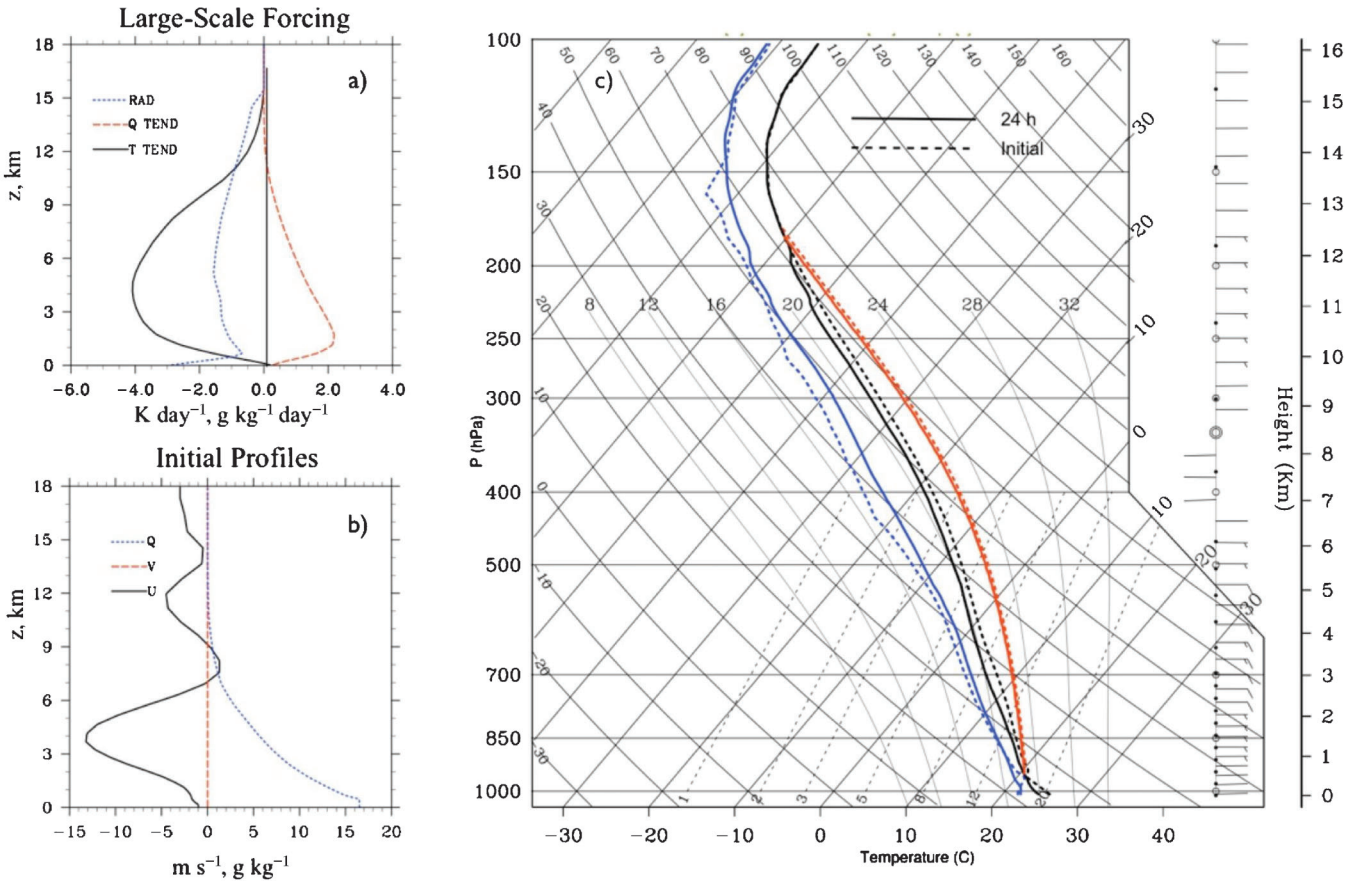

Figure 1. Prescribed (a) large-scale advective (T TEND) and radiative (RAD) cooling, and advective moistening (Q TEND) rates; (b) zonal (U) and meridional (V) wind components, and water vapor mixing ratio (q); (c) initial (dashed lines) and 24-hours-later (solid lines) skew-T diagram showing temperature (black lines), dew point temperature (blue lines), moist adiabat starting at the level of free convection (red lines), and wind speed and direction (barbs).

Table 1 Summary of the numerical experiments used in this study.

Simulation	Grid size $N_x \times N_y \times N_z$	Horizontal Grid spacing $\Delta x = \Delta y$ (m)	Vertical grid spacing Δz_{min} - Δz_{max} (m)
BASE	2048 × 2048 × 256	100	50 - 300
H200	1024 × 1024 × 256	200	50 - 300
H400	512 × 512 × 256	400	50 - 300
H800	256 × 256 × 256	800	50 - 300
H1600	128 × 128 × 256	1600	50 - 300
L64	256 × 256 × 64	800	75 - 500
NOEVP	1024 × 1024 × 256	200	50 - 300

there was only minimal drift of the thermodynamic sounding from the idealized GATE sounding at the end of the 24-hour run. The thermodynamic sounding exhibits a substantial amount of convective available potential energy (CAPE), i.e., about 1200 J kg^{-1}, and a very small amount of convective inhibition (CIN), i.e., less than 3 J kg^{-1}. The zonal mean wind exhibits strong easterlies in the lower troposphere, with a maximum wind speed of 13 m s^{-1} at the 4 km level.

As summarized in Table 1, we have examined the sensitivity of our results to 1) horizontal grid spacing, 2) vertical grid spacing, and 3) evaporation of precipitation. Each run lasted for a period of 24 hours with the same numerical domain of 204.8 km wide in both horizontal directions and about 27 km in the vertical. In the horizontal-grid sensitivity runs, the horizontal grid spacing was varied over a rather wide range, from LES-like 100 m (BASE) to CRM-like 800-1600 m. The 256-level vertical grid used in these runs had a spacing of 50 m below 1200 m, linearly increasing to 100 m at 5,000 m, staying constant at 100 m up to the 18,000 m level, and then linearly increasing to 300 m at the domain top. In the vertical resolution sensitivity run L64, the horizontal grid spacing was 800 m, and the vertical grid was degraded to a CRM-like 64-level grid with a grid spacing that increases smoothly from 75 m near the surface to 500 m above 3000 m. The NOEVP run was similar to the H200 high-resolution run except that the evaporation of precipitation was switched off, which effectively eliminated the cold pools associated with convection. All runs were performed with a 2 s time step. The resolved turbulent motion was initiated by adding random perturbations with amplitude of 0.1 K to the initial temperature field at all grid points below the 300 m level. No perturbations were added at later times.

All runs were performed on the IBM Blue Gene/L "New York Blue" supercomputer at the New York Center for Computational Sciences. The most expensive run, the benchmark BASE, was performed using 2048 processors, took about six days of wall-clock time to complete, and produced about 5.5 TB of output[2].

4. The benchmark simulation

The evolution of convection in the benchmark BASE run is illustrated by the time series of horizontally averaged non-precipitating cloud liquid/ice condensate, as shown in Fig. 2. A very pronounced 'spin-up' or transition period is evident during the first 6 simulated hours. During the spin-up, shallow boundary layer clouds appear just after one simulation hour. The shallow cloudy layer gradually deepens until an explosive transition to deep cumulus convection occurs near hour 6. A nearly steady deep cumulus regime is established by hour 12. This regime is characterized by a trimodal vertical distribution of clouds similar to that often observed in the Tropics (Johnson et al. 1999), in which shallow and deep convective cloud maxima are accompanied by a cumulus congestus maximum in the mid-troposphere near the freezing level.

Figure 3 shows the time evolution of horizontally averaged latent and sensible heat fluxes, precipitation rate at the surface along with the CAPE, CIN, and cloud amount. The CAPE and CIN were computed from the domain-average thermodynamic profiles assuming pseudo-adiabatic ascent with the departure point near the surface. After the spin-up, precipitation is quasi-steady, oscillating between 9 and 13 mm day^{-1}. The cloud cover is in the 25-30% range. The latent and sensible heat fluxes appear to be close to a statistically steady state with a relatively small upward trend; it would be unreasonable to expect that a full equilibrium could be reached in just a few simulated hours. During the spin-up, the large-scale forcing was continuously applied without any response from deep convection; this resulted in

[2] The dataset is stored at the CMMAP digital library and can be downloaded from www.cmmap.org.

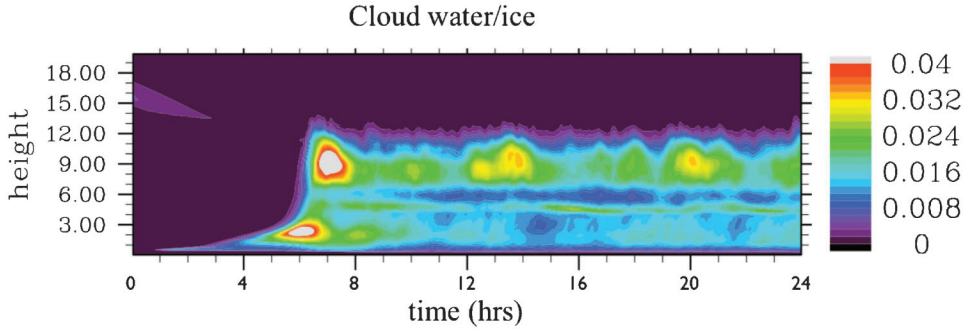

Figure 2. The evolution of horizontally averaged cloud liquid/ice water mixing ratio profile ($\times 10^{-3}$ kg kg^{-1}) in the benchmark BASE run.

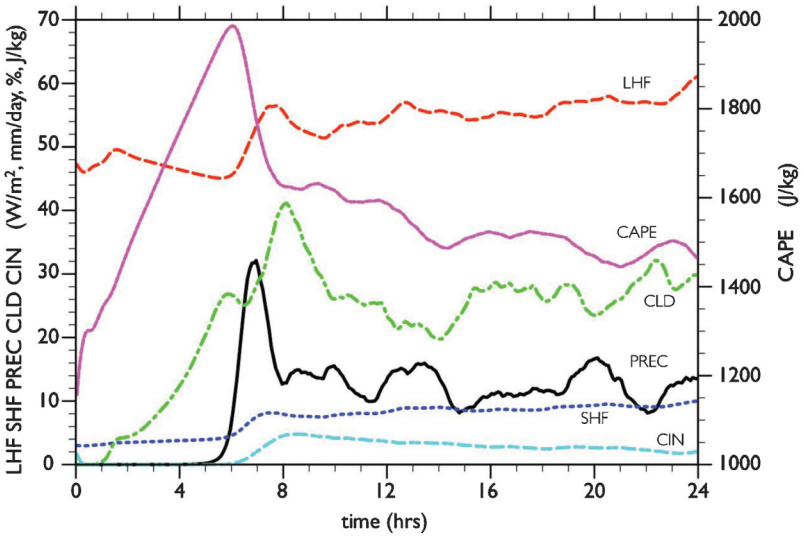

Figure 3. Time evolution of horizontally averaged precipitation rate (PREC, mm day^{-1}), latent (LHF, W m^{-2}) and sensible (SHF, W m^{-2}) surface heat fluxes, cloud cover (CLD, %), CAPE (J kg^{-1}), and CIN (J kg^{-1}) in the benchmark run BASE.

an almost doubling of the value of CAPE from 1200 to 2000 J kg^{-1} during the first six hours. This CAPE build-up is followed by a burst of deep convection, which removes about half of the additional CAPE. Subsequently, the CAPE approaches equilibrium, at about 1500 J kg^{-1}. During the burst, the CIN increases from virtually zero to about 5 J kg^{-1} due to stabilization of the low troposphere by compensating subsidence. After the burst, CIN also trends down towards equilibrium. Previous studies (Mapes 2000; Kuang and Bretherton 2006) have suggested that CIN plays an important role in regulating the cloud-base mass-flux.

5. The cold pools and tri-modal cloud distribution

This study supports previous findings that cold pools play a very important role in organizing deep convection on the mesoscale and in triggering new deep convective cells (Tompkins 2001; Kuang and Bretherton 2006; Khairoutdinov and Randall 2006). Figure 4 presents a visualization of the cloud scene[3] over the whole 205 × 205 km^2 domain at hour 13. Note that the domain size is comparable to the grid-cell size of a typical GCM and, hence, the scene illustrates the complexity of representing the statistical effects of clouds over the scales unresolved by GCMs. One can see individual deep clouds and cloud systems dominated by extensive anvils and surrounded by smaller congestus and shallow clouds. Due to the vertical shear of the zonal wind, the deep convection tends to organize in the zonal direction producing mid-level pairs of mesocyclones; however, no squall-line developed during the simulation period, probably due to the relatively weak shear, with the low-level jet at a relatively high 4-km level (see Fig. 1). Some of the deep clouds are surrounded by arc-shaped structures, which reveal gust fronts at the edges of spreading cold pools in the PBL produced by convective downdrafts. The downdrafts are forced by the evaporative cooling and precipitation loading, and bring drier air from the free troposphere down to the PBL. This is illustrated by a

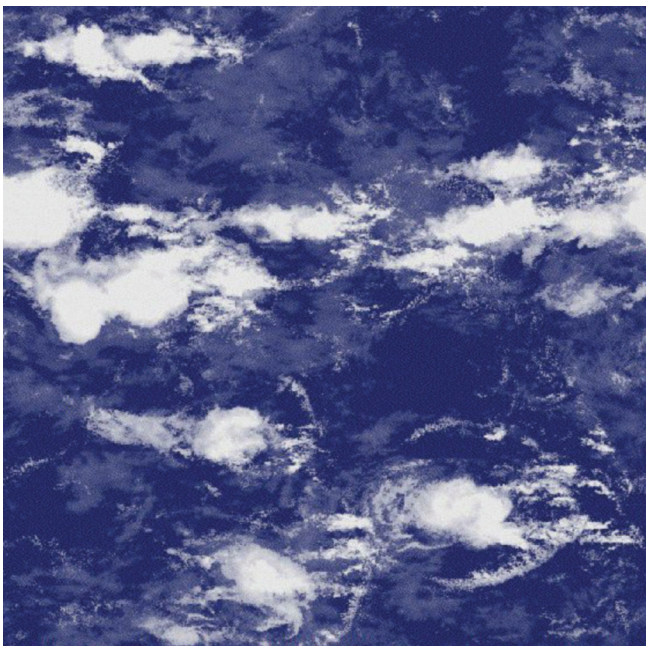

Figure 4. Visualization of simulated cloud scene over the area of 205 × 205 km^2 corresponding to hour 13 of the BASE run. The image represents visible albedo estimated from the liquid and ice water paths. The cloud arcs around some of the deep clouds are the shallow clouds lifted up by the gust fronts at the edges of spreading cold pools. The semi-transparent gray-blue areas indicate the presence of cirrus clouds, while dark-blue areas are cloud-free.

[3] The supplemental file with the animation of 24 hours of the baseline case is available as part of this publication. DOI: 10.3894/JAMES.2009.1.15.S1

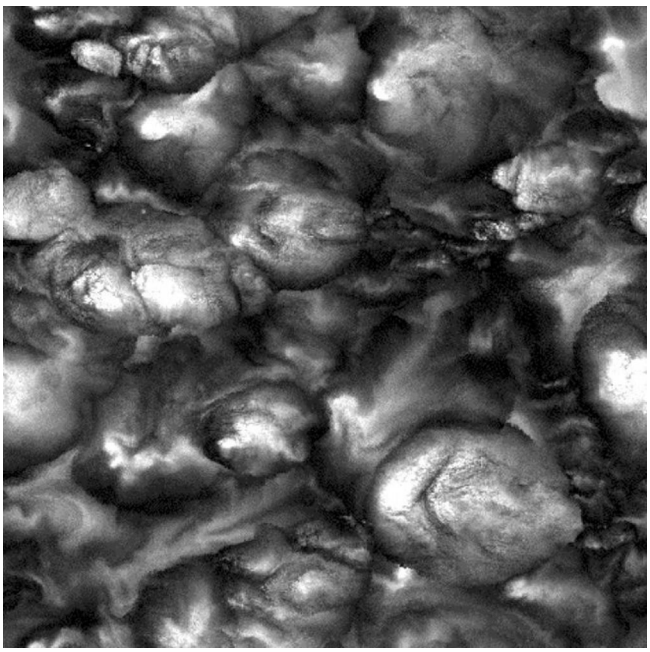

Figure 5. Water vapor mixing ratio at the lowest model layer 25 meters above the surface corresponding to the cloud scene in Fig. 4. The light-shaded areas correspond to drier air. The contrast between the darkest and lightest shading represents approximately 4 g kg^{-1} contrast in mixing ratio.

visualization of near-surface water vapor mixing ratio, shown in Fig. 5, where the newly formed cold pools as well as the pools from earlier events are clearly seen. The companion paper by Moeng et al. (2009) presents a more detailed analysis of the boundary layer properties in the benchmark run including the cold pools.

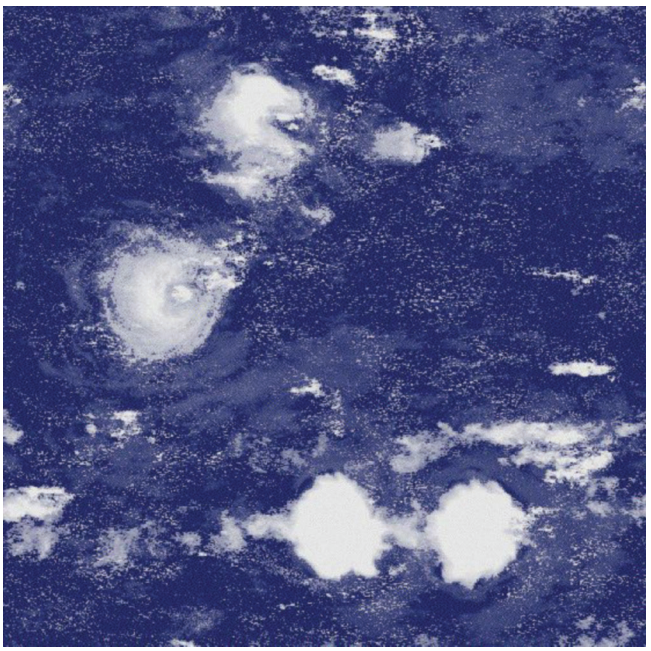

Figure 7. Visualization of simulated cloud scene over the area of 205 $\times$ 205 km^2 for the run with no evaporation of precipitation.

To illustrate the important role that cold pools may play in maintaining the tri-modal vertical distribution of clouds in Tropics, we performed the run NOEVP (see Table 1) in which cold pools were artificially diminished by switching off the evaporation of precipitation. Figure 6 illustrates the dramatic effect of such a switch-off, namely, a significant reduction of the low and congestus cloud amount. In particular, the cloud fraction associated with those types of clouds has been reduced by about a half (not shown). Figure 7 presents a visualization of a cloud scene over the

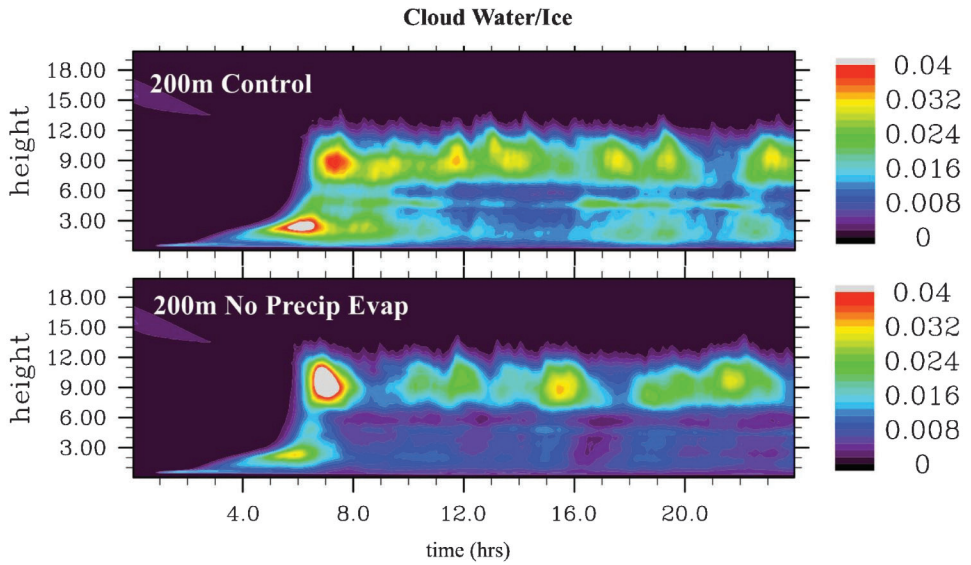

Figure 6. Evolution of horizontally averaged profile of cloud liquid/ice water mixing ratio for the control (top), and for the run with no evaporation of precipitation.

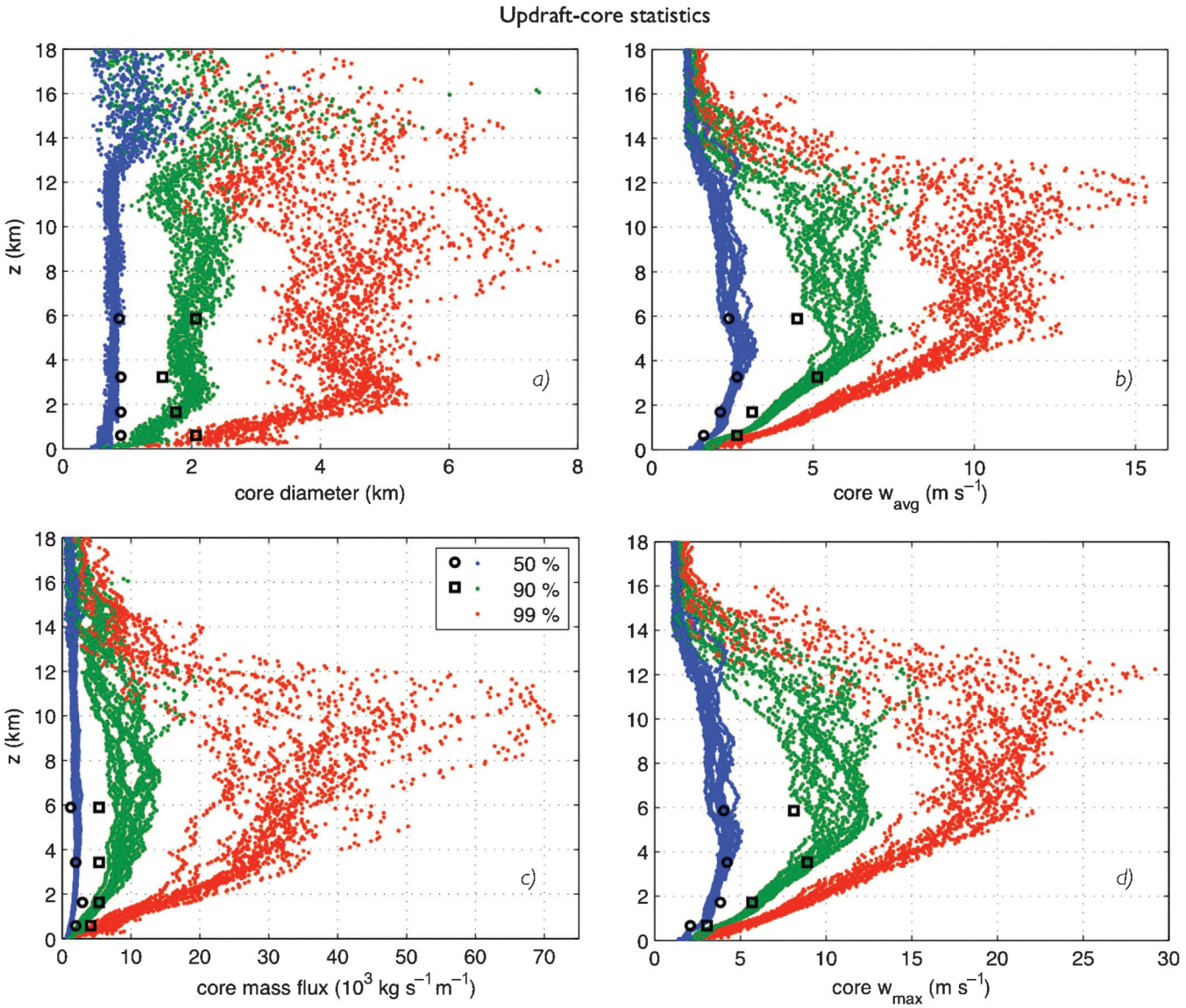

Figure 8: Vertical velocity statistics for the updraft cores: a) diameter, b) mean vertical velocity, c) core mass flux, and d) maximum vertical velocity from the last 12 hours of the BASE run (dots) and from flight data by LeMone and Zipser (1980; black circles and squares) based on GATE aircraft penetrations. A core has vertical velocity magnitude of at least 1 m s^{-1} for 500 m or more. The 50th percentile (median; blue dots), 90th percentile (10 percent are greater; green dots), and 99th percentile (1 percent are greater; red dots) are shown. For the BASE run, each plotted point represents one level at one time.

205 × 205 km^2 domain from the NOEVP run. When compared with the cloud scene from the benchmark run (see Fig. 4), the NOEVP run consists of several isolated deep towers surrounded by vast areas of sporadic shallow clouds underneath subsiding air, and very few congestus clouds, which exist very close to the deep clouds. Animations of the cloud scenes clearly show[4] that new deep clouds in the NOEVP run tend to develop at the sites of the previous deep clouds, suggesting meso-scale low-level moisture convergence over those sites. In contrast, in the benchmark BASE run, the new deep clouds tend to appear along the edges of spreading cold pools where moisture converges, which also favors the formation of shallow and congestus convection.

[4] The supplemental file with the animation is available as part of this publication.

6. Updraft and downdraft core statistics

Figures 8 and 9 show the core statistics for the updrafts and downdrafts, respectively, of average and maximum vertical velocity, core diameter, and core mass flux from BASE and from GATE observations by LeMone and Zipser (1980; further LZ80). The BASE vertical velocity fields were analyzed at hourly intervals for the last 12 hours of the simulation. Each field was analyzed as if it consisted of 2048 parallel

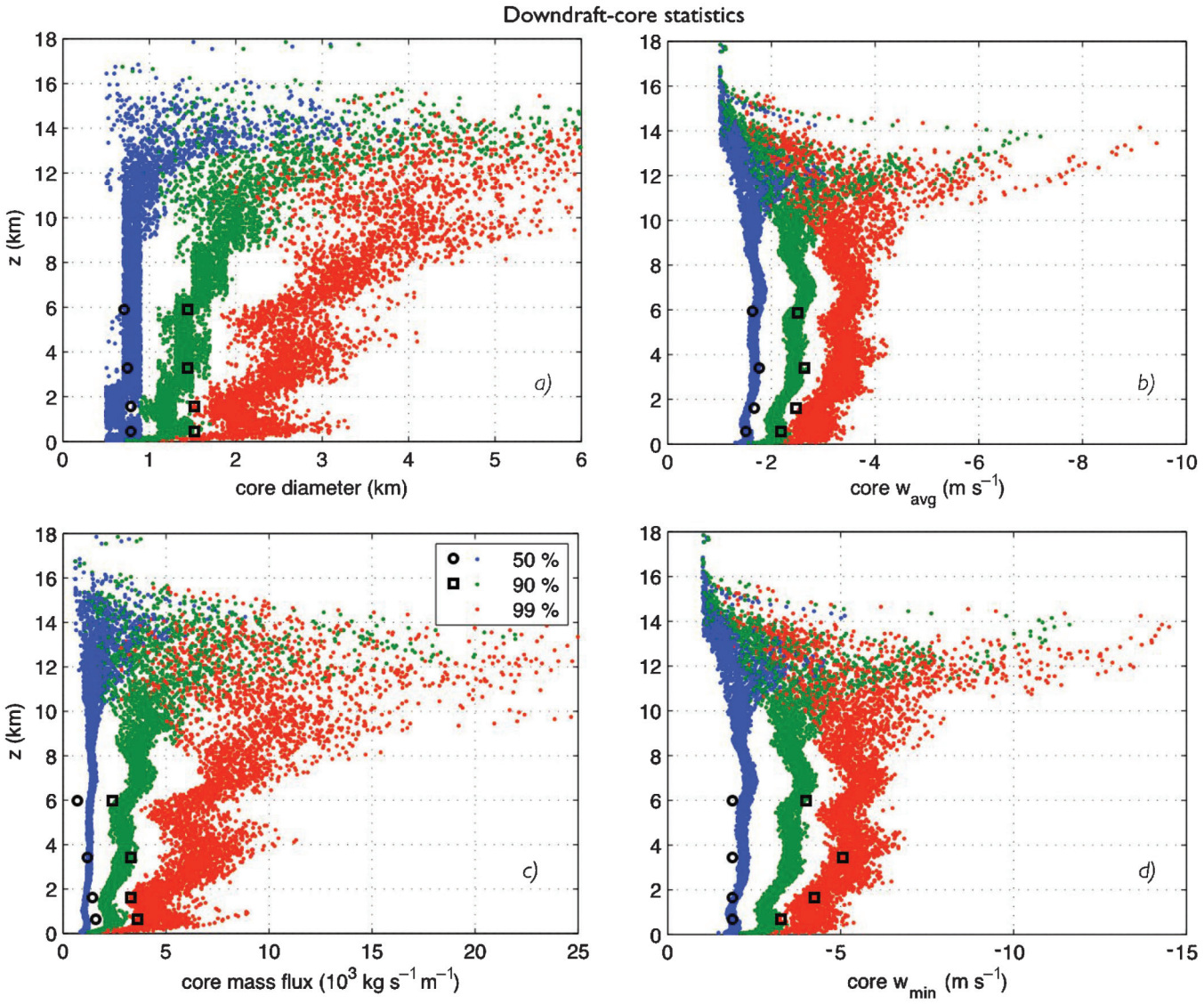

Figure 9. Same as Fig. 8, but for the downdraft cores.

aircraft flight legs of length 204.8 km in the zonal direction at each model level. Each plotted point from BASE represents the median, 90th percentile, or 99th percentile value for a particular updraft or downdraft core property for one level at one time. The results above 12 km are due to gravity waves, not convective updrafts, which is evident from the plots of scalar fluxes (for example, see Fig. 11e).

The comparison shows very good agreement with the observations, especially for the updraft and downdraft cores of median strength. Additional analysis shows that the stronger updrafts have larger diameters, which supports the notion that bigger clouds entrain relatively less and, hence, are more buoyant (e.g., Kuang and Bretherton 2006; Khairoutdinov and Randall 2006). There is a discrepancy for the maximum velocities in the 90th-percentile downdrafts, with smaller values in the simulation, although the average downdraft velocities are more consistent.

For the 90th-percentile updraft cores, there is some disagreement between the simulated and observed average vertical velocities and their maximum values between the 3 and 6 km levels, with larger values in the simulation. These discrepancies may be within the uncertainty of the LZ80 statistics, which are based on a relatively small number of aircraft penetrations compared to the much larger number of samples computed from the model output, and which as the result may underestimate the number of stronger but less frequent updrafts.

7. Sensitivity to grid resolution

7.1. Horizontal grid spacing

The goal of the horizontal-resolution sensitivity study was 1) to study the impact of using a much coarser horizontal grid

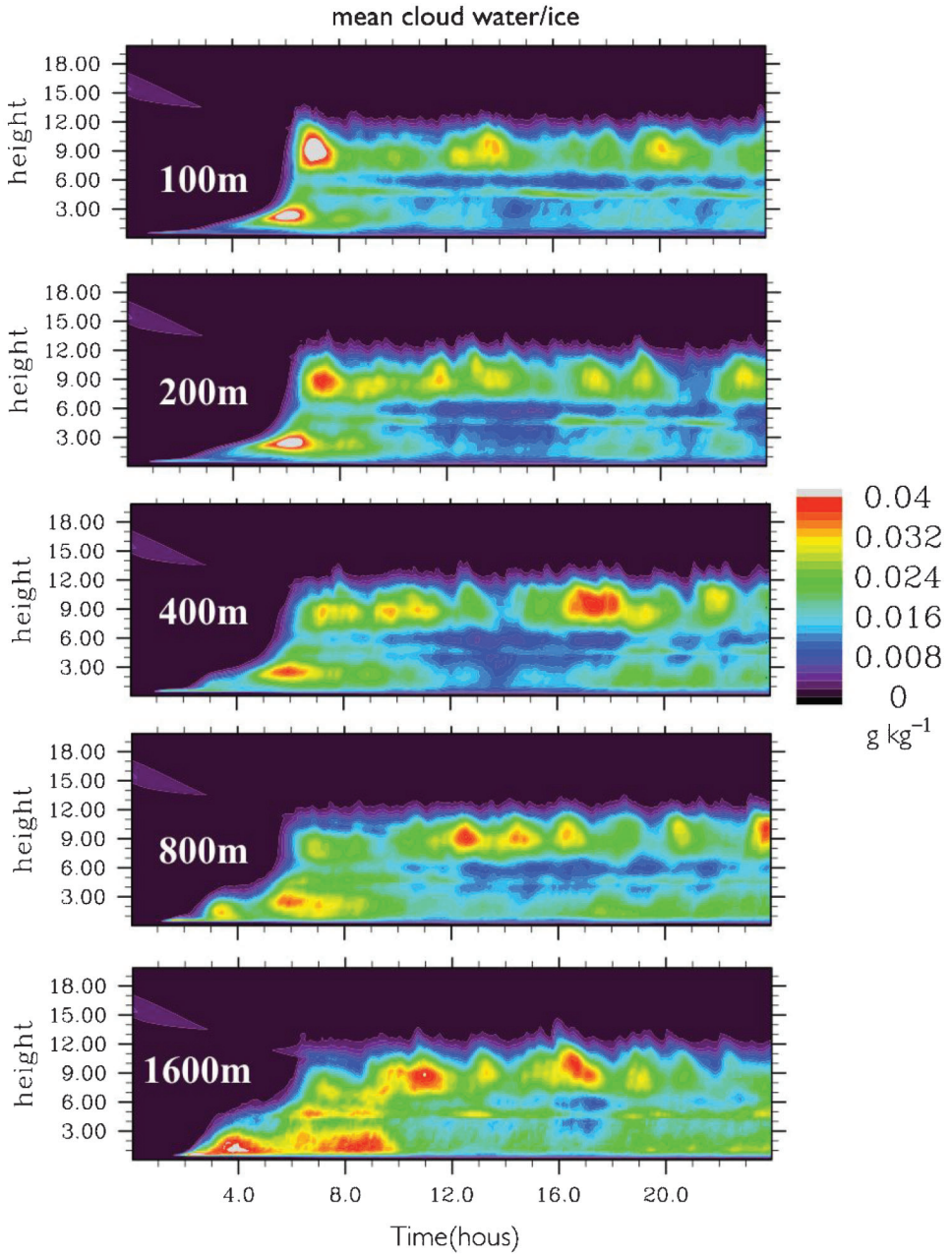

Figure 10. The evolution of horizontally averaged cloud liquid/ice water mixing ratio ($\times 10^{-3}$ kg kg^{-1}) profile in horizontal resolution sensitivity runs, from 100 m (top) up to 1600 m (bottom).

size of 1-2 km typically employed in CRM studies of deep convection, and 2) to see if there is numerical convergence of the statistical properties of convection with decreasing grid size. We performed four more simulations with horizontal grid sizes of 200 m, 400 m, 800 m, and 1600 m (see Table 1), respectively. The domain size, vertical grid, time step, initial sounding, and forcing profiles remained the same as the BASE run. The evolution of convection among the cases is broadly similar as illustrated by the time series of horizontally averaged cloud ice/liquid water profiles in Fig. 10. All cases transition to deep convection after 6 hours of simulation, although the transition in the coarse resolution runs is not as abrupt as that in the fine resolution runs. All runs clearly show the tri-modal vertical distribution of clouds, although the cumulus congestus maximum tends to be less pronounced as the resolution degrades (with the exception of the coarsest 1600 m run).

Figure 11 presents the vertical profiles of several horizontally averaged quantities averaged over the last 12 hours of the simulation period. The low clouds tend to occupy larger fractions of the area (Fig. 11a) and together contain more cloud water as the grid spacing increases (Fig. 11b). In

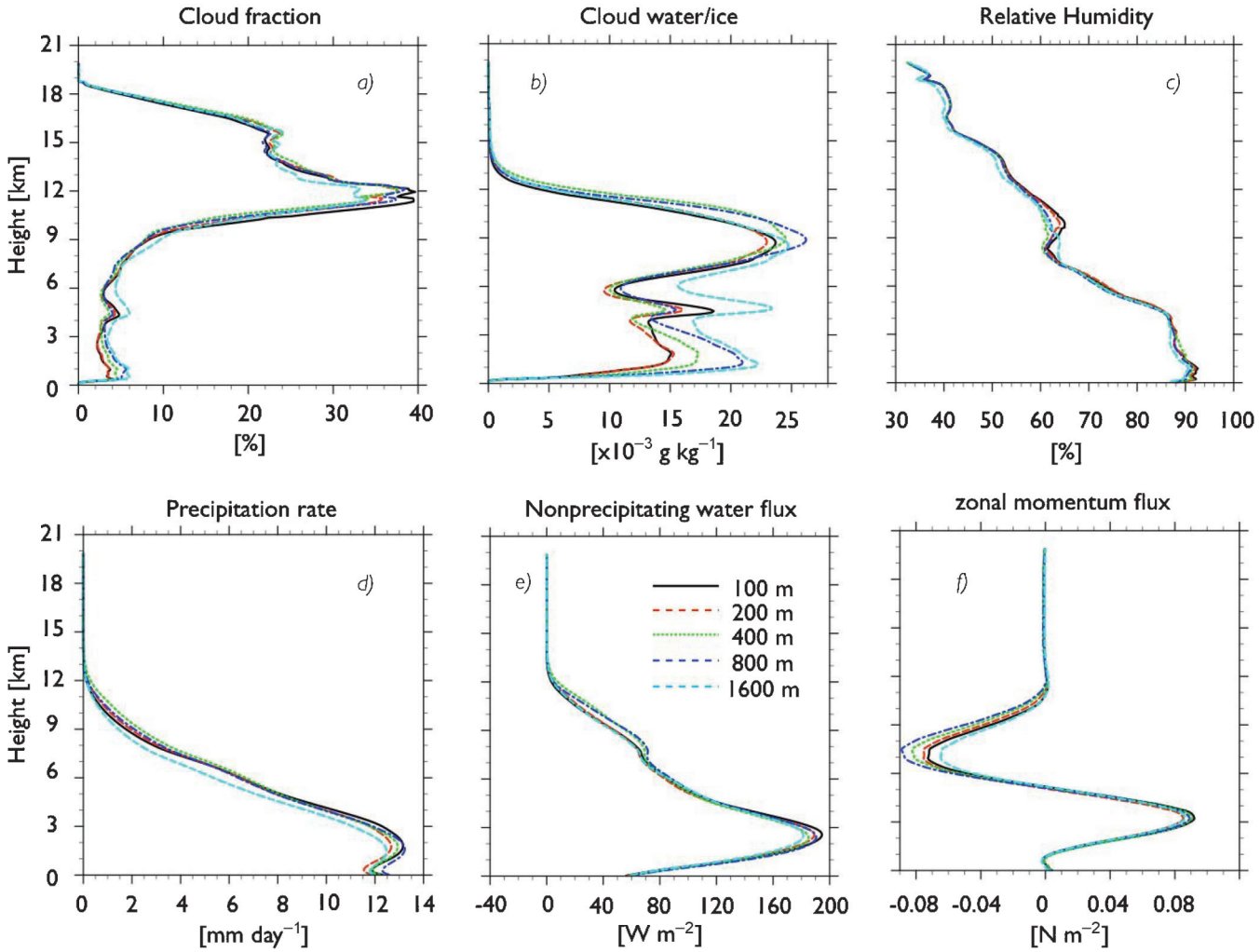

Figure 11. Comparison of vertical profiles of horizontally averaged a) cloud fraction, b) liquid/ice cloud water mixing ratio, c) relative humidity with respect to liquid water, d) precipitation flux, e) flux of non-precipitating, water+condensate, water, and f) flux of zonal momentum averaged over the last 12 hours of the benchmark 100 m LES run and horizontal-spacing sensitivity runs.

contrast, the anvil area fraction associated with deep clouds does not show clear dependence on the resolution. This may be expected because deep clouds are bigger than shallow and congestus clouds, and, therefore, their properties are less sensitive to grid resolution. Relatively large cloud cover with very low ice content above the anvil cover maximum at 12 km is due to thin cirrus clouds associated with gravity waves excited by deep convection. The profile of relative humidity (with respect to liquid water saturation mixing ratio; Fig. 11c) does not vary significantly with horizontal resolution although there is a subtle tendency for the PBL as well as the anvil layer to be more humid in the higher resolution runs. The vertical fluxes of all prognostic fields are also quite robust, as illustrated by the precipitation sedimentation flux (Fig. 11d), fluxes of total non-precipitating (vapor plus condensate and small ice) water (Fig. 11e) and zonal momentum (Fig. 11f). The near equilibrium values of CAPE, CIN, precipitation rates, and surface latent and sensible fluxes (not shown) are also all in close agreement with the benchmark case.

Perhaps the good agreement in such bulk quantities as fluxes, cloud fraction, and mean thermodynamics profiles, among the runs with horizontal grid sizes varying by one order of magnitude, is a consequence of the thermodynamic constraints imposed by the prescribed steady large-scale forcing. Also, the bulk of vertical transport in this case is done by deep heavily precipitating cloud systems that have an associated mesoscale circulation tens of kilometers in size (see Fig. 4), which is well represented even on a grid with 1 km spacing. However, there are rather significant changes in how clouds 'work' as resolution degrades, as illustrated by the cloudy updraft core statistics in Fig. 12. The updraft core is defined as cloudy grid points where vertical velocity exceeds 1 m s^{-1}. As the horizontal grid spacing becomes larger, the core updrafts become weaker (Fig. 12a). Also, the excess of total water over the environment in updraft cores

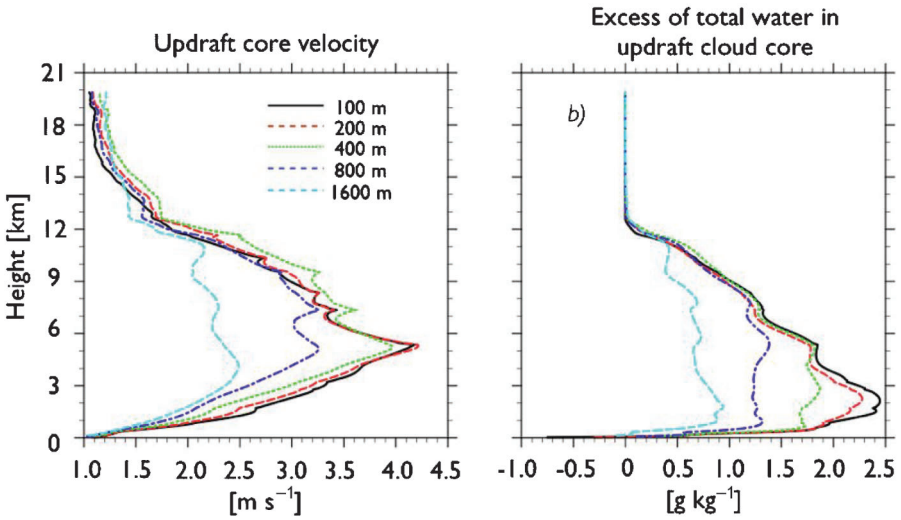

Figure 12. Same as Fig. 11, but for a) updraft-core mean vertical velocity and b) average excess of total non-precipitating water in updraft cores over the horizontal mean values. The updraft cores were defined as cloudy points with vertical velocity exceeding 1 m s^{-1}.

diminishes with reduced resolution (Fig. 12b). The reduction begins near the cloud base and hence is most likely due to reduced variance of water vapor in the PBL, not due to changes in cloud entrainment. However, the total water flux (see Fig. 11e) and surface evaporation flux (not shown) do not vary with resolution; therefore, to maintain them, the fractional core updraft area should increase with increased grid spacing (see Fig. 11e) to compensate for weaker and less moist updrafts. This is especially the case in the lower troposphere where the vertical transport by smaller, hence more sensitive to resolution, low-level clouds takes place. The increase in low-troposphere cloud fraction also manifests itself in increased horizontally averaged cloud/ice water (see Fig. 11b) for increased grid spacing. Large differences in low-level cloud fraction was also reported by Blossey et al. (2009) who studied a completely different case and compared 100 m LES results to a coarse 4 km horizontal grid spacing CRM result.

Regarding the issue of convergence of the results as horizontal resolution increases, the results of 100 and 200 m horizontal grid spacing do seem very similar to each other, which is illustrated by Fig. 12, and also by numerous other cloud statistics not shown here. The convergence at 100-200 m range of horizontal grid spacing is supported by the notion that the Kolmogorov inertial sub-range of turbulence spectra in the PBL seem to extend up to about half a kilometer scale, as shown by Moeng et al. (2009, their Fig. 8). The SGS parameterization used by SAM is largely based on scaling arguments that assume that the grid spacing is within the Kolmogorov sub-range. Therefore, perhaps it is not a coincidence that the 100 and 200 m runs produce similar statistics. Note that running the model at 200 m rather than 100 m spacing means saving at least a factor of four in terms of the CPU time, which is significant considering the large computational expense (about 300,000 CPU hours) of the benchmark run.

7.2. Vertical grid spacing

The benchmark BASE run was performed using a grid with 256 vertical grid levels, which is a rather large number of levels compared to the number of levels typically employed by CRMs of deep convection. To see the effect of higher vertical resolution on the results of SAM with a typical CRM horizontal grid size of O(1 km), we repeated the H800 run (800 m horizontal grid spacing; see Table 1) with a more typical CRM vertical grid with only 64 levels (case L64). The L64 grid had only 9 levels in the lowest 1000 m with the grid spacing increasing from 75 m near the surface, to about 200 m at 1000 m, and then to 500 m above 3500 m. The top of the domain was kept the same as that in the H800 run.

Figure 13 compares the time evolution of the horizontally averaged cloud ice/liquid water profiles for the benchmark BASE, control H800, and L64 runs. Overall, the simulations exhibit similar behavior with two important exceptions. First, it is clear that the tri-modal vertical distribution of clouds so well represented in the BASE and the H800 runs has virtually disappeared in L64. Secondly, L64 overestimates the water content and fraction (not shown) of low tropospheric clouds and, to a lesser degree, deep clouds, although the vertical fluxes of these scalars are rather well simulated (not shown). Thus, we conclude that in order for SAM to minimize errors in representation of deep tropical convection using a conventional O(1 km) horizontal grid spacing, the vertical grid should have a minimal spacing of 50-100 m below the 500 mb level.

8. Summary

In this paper, we present an LES of deep tropical convection over a large horizontal domain of 205 × 205 km^2, which is comparable to a typical grid cell size in a global climate model. It is a 24-hour long simulation forced with large-

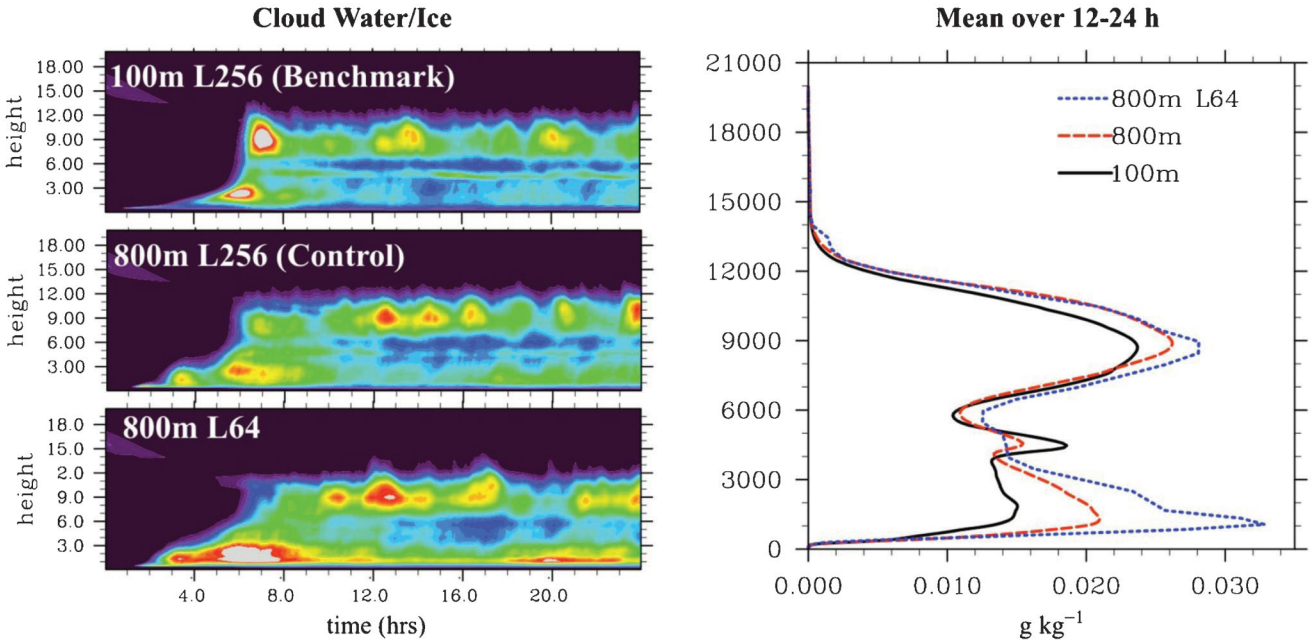

Figure 13. (Left panel) Comparison of the evolution of horizontally averaged cloud liquid/ice water mixing ratio profile in the benchmark 100 m LES (top), and in the 800 m horizontal grid spacing and 256 levels (middle) and 64 levels (bottom). (Right panel) The profiles averaged over the last 12 hours of each simulation.

scale tendencies derived from mean conditions during the GATE Phase III field experiment. The benchmark simulation uses 2048 × 2048 × 256 grid points with horizontal grid spacing of 100 m and vertical grid spacing in the range from 50 m in the PBL to 100 m in free troposphere. The LES of deep tropical convection was performed as part of the CMMAP (Center for Multicsale Modeling of Atmospheric Processes) project to advance our understanding of cloud interactions with the PBL turbulence, with the environment, and among different cloud scales, with the goal of improving parameterizations in GCMs and CRMs.

The simulation reaches a near equilibrium deep convection regime in 12 hours. The simulated vertical cloud distribution exhibits a tri-modal vertical distribution of deep, middle and shallow clouds similar to that often observed in Tropics. We demonstrated the role that the cold pools play in maintaining the tri-modal cloud distribution by performing a sensitivity experiment in which cold pools are suppressed by switching off the evaporation of precipitation. Without cold pools the shallow and congestus cloud amounts are significantly reduced. The deep clouds also behave differently from the benchmark, with isolated deep towers surrounded by vast areas of shallow convection and just a few congestus clouds. Unlike the benchmark in which the new deep clouds tend to appear along the edges of spreading cold pools where the moisture converges, the deep clouds in no-cold-pool simulation tend to reappear at the sites of the previous deep clouds.

For the first time, a simulation's vertical velocity statistics in updraft and downdraft cores has been unambiguously compared to the LeMone and Zipser (1980) aircraft observations. The comparisons of the cores' average vertical velocity, maximum vertical velocity, diameter, and mass flux, are generally very good. The largest discrepancies are found in the strongest updraft-core average and the updraft-core maximum vertical velocities between 3 and 6 km.

We use the benchmark LES to verify results from a series of runs with progressively coarser grid spacings of 200, 400, 800, and 1600 m, respectively. The evolution of convection remains similar, with all runs showing the tri-modal top-heavy vertical distribution of clouds. The near equilibrium values of CAPE, CIN, precipitation rates, and surface latent and sensible fluxes are also in close agreement with the LES benchmark. However, despite good agreement in these bulk quantities, there are rather significant differences in the statistical behavior of the cloudy updraft cores. The simulated results exhibit convergence only between the LES benchmark and the 200 m grid spacing run, perhaps because both runs resolve the Kolmogorov inertial sub-range of turbulence. We also test the effect of higher vertical resolution by comparing two runs with 256 and 64 vertical grid levels. The coarser vertical grid fails to produce the tri-modal vertical distribution of clouds and also greatly overestimates the water content and fraction of the shallow and congestus clouds.

Acknowledgments: This study was supported by the National Science Foundation's Science and Technology Center for Multi-scale Modeling of Atmospheric Processes (CMMAP), managed by Colorado State University under cooperative agreement No. ATM-0425247. All computations were performed on the IBM Blue Gene/L 'New York Blue'

supercomputer at the New York Center for Computational Sciences (NYCCS) which is a joint venture of Stony Brook University and Brookhaven National Laboratory.

References

Blossey P. N., C. S. Bretherton, and M. C. Wyant 2009: Subtropical low cloud response to a warmer climate in a parameterized climate model. Part II: Column modeling with a cloud resolving model. *J. Adv. Model. Earth Syst.*, **Vol. 1**, Art. #8, 14 pp., doi: 10.3894/JAMES.2009.1.8.

Bryan, G. H., J. C. Wyngaard, and J. M. Fritsch, 2003: Resolution requirements for the simulation of deep moist convection. *Mon. Wea. Rev.*, **131**, 2394–2416, doi: 10.1175/1520-0493(2003)131<2394:RRFTSO>2.0.CO;2.

Deardorff, J. W., 1980: Stratocumulus-capped mixed layers derived from a three-dimensional model. *Bound. Layer Meteorol.*, **18**, 495–527, doi: 10.1007/BF00119502.

Fu, Q., S. K. Krueger, and K. N. Liou, 1995: Interactions of radiation and convection in simulated tropical cloud clusters. *J. Atmos. Sci.*, **52**, 1310–1328, doi: 10.1175/1520-0469(1995)052<1310:IORACI>2.0.CO;2.

Grabowski, W. W., X. Wu, M. W. Moncrieff, and W. D. Hall, 1998: Cloud-resolving modeling of cloud systems during Phase III of GATE. Part II: Effects of resolution and the third spatial dimension.*J. Atmos. Sci.*, **55**, 3264–3282, doi: 10.1175/1520-0469(1998)055<3264:CRMOCS>2.0.CO;2.

IPCC, 2007: Climate Change 2007: The Physical Science Basis. Cambridge University Press, 800 pp.

Johnson, R. H., T. M. Rickenbach, S. A. Rutledge, P. E. Ciesielski, and W. H. Schubert, 1999: Trimodal characteristics of tropical convection. *J. Climate*, **12**, 2397–2418, doi: 10.1175/1520-0442(1999)012<2397:TCOTC>2.0.CO;2.

Khairoutdinov, M. F., and D. A. Randall, 2003: Cloud resolving modeling of the ARM summer 1997 IOP: Model formulation, results, uncertainties and sensitivities. *J. Atmos. Sci.*, **60**, 607–625, doi: 10.1175/1520-0469(2003)060<0607:CRMOTA>2.0.CO;2.

Khairoutdinov, M. F., and D. A. Randall, 2006: High-resolution simulation of shallow-to-deep convection transition over land. *J. Atmos. Sci.*, **63**, 3421–3436, doi: 10.1175/JAS3810.1.

Klemp, J. B., and R. B. Wilhelmson, 1978: The simulation of three-dimensional convective storm dynamics. *J. Atmos. Sci.*, **35**, 1070–1096, doi: 10.1175/1520-0469(1978)035<1070:TSOTDC>2.0.CO;2.

Krueger, S. K., 1988: Numerical simulation of tropical cumulus clouds and their interactions with the subcloud layer. *J. Atmos. Sci.*, **45**, 2221–2250, doi: 10.1175/1520-0469(1988)045<2221:NSOTCC>2.0.CO;2.

Kuang, Z., and C. S. Bretherton, 2006: A Mass-flux scheme view of a high-resolution simulation of a transition from shallow to deep cumulus convection. *J. Atmos. Sci.*, **63**, 1895–1909, doi: 10.1175/JAS3723.1.

LeMone, M. A., and E. J. Zipser, 1980: Cumulonimbus Vertical Velocity Events in GATE. Part I: Diameter, Intensity and Mass Flux. *J. Atmos. Sci.*, **37**, 2444–2457, doi: 10.1175/1520-0469(1980)037<2444:CVVEIG>2.0.CO;2.

Mapes, B. E., 2000: Convective inhibition, subgrid-scale triggering energy, and stratiform instability in a toy tropical wave model. *J. Atmos. Sci.*, **57**, 1515–1535, doi: 10.1175/1520-0469(2000)057<1515:CISSTE>2.0.CO;2.

Moeng, C.-H., M. A. LeMone, M. F. Khairoutdinov, S. K. Krueger, P. Bogenschutz, and D.A. Randall, 2009: The tropical marine boundary layer under a deep convection system: a large-eddy simulation study. *J. Adv. Model. Earth Syst.*, **Vol. 1**, Art. #16, 13 pp., doi: 10.3894/JAMES.2009.1.16.

Moeng, C.-H., and J. C. Wyngaard, 1988: Spectral analysis of large-eddy simulations of the convective boundary layer. *J. Atmos. Sci.*, **45**, 3573–3587, doi: 10.1175/1520-0469(1988)045<3573:SAOLES>2.0.CO;2.

Nasuno, T., H. Tomita, S. Iga, H. Miura, and M. Satoh, 2007: Multiscale Organization of Convection Simulated with Explicit Cloud Processes on an Aquaplanet. *J. Atmos. Sci.*, **64**, 1902–1921, doi: 10.1175/JAS3948.1.

Petch, J. C., A. R. Brown, and M. E. B. Gray, 2002: The impact of horizontal resolution on the simulations of convective development over land. *Quart. J. Roy. Meteor. Soc*, **128**, 2031–2044, doi: 10.1256/003590002320603511.

Randall, D. A., M. Khairoutdinov, A. Arakawa, and W. Grabowski, 2003: Breaking the cloud parameterization deadlock. *Bull. Amer. Meteor. Soc.*, **84**, 1547–1564, doi: 10.1175/BAMS-84-11-1547.

Redelsperger, J.-L., and G. Sommeria, 1986: Three-dimensional simulation of a convective storm: Sensitivity studies on subgrid parameterization and spatial resolution. *J. Atmos. Sci.*, **43**, 2619–2635, doi: 10.1175/1520-0469(1986)043<2619:TDSOAC>2.0.CO;2.

Siebesma, A. P. and Coauthors, 2003: A large-eddy simulation intercomparison study of shallow cumulus convection. *J. Atmos. Sci.*, **60**, 1201–1219, doi: 10.1175/1520-0469(2003)60<1201:ALESIS>2.0.CO;2.

Stevens, B. and Coauthors, 2005: Evaluation of large-eddy simulations via observations of nocturnal marine stratocumulus. *Mon. Wea. Rev.*, **133**, 1443–1462, doi: 10.1175/MWR2930.1.

Tao, W.-K. and S.-T. Soong, 1986: A study of the response of deep tropical clouds to mesoscale processes: Three-dimensional numerical experiments. *J. Atmos. Sci.*, **43, 17**, 2653–2676, doi: 10.1175/1520-0469(1986)043<2653:ASOTRO>2.0.CO;2.

Tompkins, A. M., 2001: Organization of tropical convection in low vertical wind shears: the role of cold pools. *J. Atmos. Sci.*, **58**, 1650–1672, doi: 10.1175/1520-0469(2001)058<1650:OOTCIL>2.0.CO;2.

Xu, K.-M., A. Arakawa, and S. K. Krueger, 1992: The macroscopic behavior of cumulus ensembles simulated by a cumulus ensemble model. *J. Atmos. Sci.*, **49**, 2402–2420, doi: 10.1175/1520-0469(1992)049<2402:TMBOCE>2.0.CO;2.